Original Article

The ubiquitin ligase RCBTB2 regulates aggrephagy and inhibits prostate cancer progression by targeting GPAA1 for degradation

Ren Mo^{1,2*}, Ning Chi^{1,2*}, Jianjun Du², Xinhua Li², Weihang Guo², Haozhe Li², Jiawei Wang², Chuanhai Cai², Sanxiang Li^{1,2}, Chunxiao Liu¹

¹Department of Urology, Zhujiang Hospital, Southern Medical University, Guangzhou, Guangdong, China; ²Department of Urology, Inner Mongolia People's Hospital, Inner Mongolia Urological Institute, Hohhot, Inner Mongolia, China. *Equal contributors.

Received April 30, 2025; Accepted September 19, 2025; Epub October 15, 2025; Published October 30, 2025

Abstract: Background: Prostate cancer (PCa) ranks among the most prevalent malignant tumors affecting the male genitourinary system, presenting a considerable danger to health and human life. Increasing evidence indicates that the ubiquitin-proteasome pathway is essential in both the development and management of PCa. Methods: Differential expressed genes were screened by integrating the TCGA and GEO databases, and their expression was validated in the HPA dataset. An RCBTB2 overexpression cell line was constructed, and its effects on cellular behavior were analyzed using CCK-8, scratch assay, Transwell, and immunofluorescence staining. A nude mouse model was established to evaluate the tumor-suppressive effects. Furthermore, the interaction between RCBTB2 and GPAA1 was confirmed through multi-omics analysis, co-immunoprecipitation, and immunofluorescence co-localization experiments. GPAA1 knockdown cell lines were then constructed to observe changes in cellular phenotypes. Results: The expression of RCBTB2 was significantly negatively correlated with the malignancy of PCa. Overexpression of RCBTB2 notably inhibited DU145 cell proliferation, migration, invasion, and EMT, as well as reduced the growth of xenograft tumors in nude mice. Multi-omics analysis revealed that RCBTB2 promoted the ubiquitin-mediated degradation of GPAA1 (protein downregulation without changes in mRNA levels), and experiments confirmed their direct interaction. Furthermore, GPAA1 knockdown suppressed the malignant biological behaviors of PCa cells and reduced the expression of aggrephagy-related factors such as p62. Conclusion: This study for the first time unveils the molecular mechanism by which RCBTB2 inhibits PCa progression through ubiquitination-mediated degradation of GPAA1. It provides a novel target for protein homeostasis-based therapy, with promising clinical value.

Keywords: Prostate cancer, RCBTB2, ubiquitination, GPAA1

Introduction

Prostate cancer (PCa) is a common malignancy affecting the male reproductive system. In recent years, with changes in dietary habits and other risk factors, the incidence of PCa has rapidly increased, with over 1.4 million new cases and more than 370,000 deaths annually worldwide. The 5-year survival rate for advanced PCa remains dismal, staying below 30% [1, 2]. Histologically, PCa is characterized as adenocarcinoma, predominantly with luminal phenotypes and a lack of basal cells [3]. PCa exhibits a prolonged natural disease course, necessitating different treatments based on tumor

stage and invasiveness during its progression. PCa treatment approaches encompass active monitoring, radiation therapy, androgen deprivation therapy (ADT), and radical prostatectomy. However, most PCa patients progress to metastatic castration-resistant prostate cancer (CRPC) after surgical or pharmacological castration through ADT, accompanied by a median survival duration less than 15 months during this phase [4-6]. Therefore, exploring the molecular mechanisms underlying PCa progression, developing novel targeted therapies, and optimizing sequential treatment strategies are pivotal for improving survival and quality of life for patients with advanced PCa.

Tumorigenesis and progression are complex processes involving multiple factors such as gene mutations, chromosomal abnormalities, gene copy number variations, and epigenetic modifications, all of which are precisely regulated by various intracellular proteins [7]. Among these, the ubiquitin-proteasome system is vital for preserving and managing cellular homeostasis. This encompasses critical biological functions like cell cycle progression, repair of DNA damage, cellular metabolism regulation, and signal transduction [8, 9]. Ubiquitination is a dynamic and reversible posttranslational modification that attaches ubiquitin molecules to proteins to control the fate of target proteins or protein-protein interactions [10]. Increasing evidence has demonstrated that ubiquitination and deubiquitination are key contributors to prostate cancer (PCa) progression. For example, the E3 ubiquitin ligase MDM2 promotes the ubiquitination and degradation of AGPS via the proteasome pathway, while AGPS enhances ferroptosis susceptibility by promoting the production of oxidized peroxisomes, thereby inhibiting the proliferation of PCa cells [11]. Research by Sun et al. revealed that NDR1 mediates the deubiquitination and degradation of PD-L1 through the deubiquitinase USP10, suppressing CD8+ T-cell infiltration and function, thus facilitating PCa immune evasion [12]. These findings not only highlight the complexity of the ubiquitination network but also provide new perspectives for targeted therapies, such as PROTAC technology, which selectively degrades target proteins via the ubiquitin-proteasome system to achieve the directed degradation of cancer-related oncoproteins [13, 14].

RCC1 and BTB domain containing protein 2 (RCBTB2), also known as CHC1L, is a gene encoding an E3 ubiquitin ligase, the protein encoded by this gene contains two C-terminal BTB/POZ domains that are associated with the regulator of chromosome condensation protein (RCC1). RCBTB2 is considered a candidate tumor suppressor gene that may exhibit loss or low expression in prostate cancer (PCa). Its functions in inhibiting cancer and promoting cilia formation position it as a viable therapeutic target [15, 16].

This study revealed that the E3 ubiquitin ligase RCBTB2 was significantly downregulated in

PCa. Overexpression of RCBTB2 reduced proliferation, migration, invasion, and the EMT process in the DU145 PCa cell line. Furthermore, transcriptomics, proteomics, and ubiquitinated proteomics analyses demonstrated that overexpression of RCBTB2 promoted the ubiquitination and degradation of GPAA1 at the protein level while having no effect on its transcriptional level. Additionally, GPAA1 knockdown reduced DU145 cell proliferation, migration, invasion, and the EMT process, as well as inhibited the expression of aggrephagy-related factors, including p62, NBR1, and CCT2.

Materials and methods

Data sources

Transcriptomic data and clinical details for prostate adenocarcinoma (PRAD) were retrieved from The Cancer Genome Atlas (TCGA) via the Genomic Data Commons (GDC) portal (https://portal.gdc.cancer.gov/). An extensive dataset comprising 534 samples were employed, comprising 483 tumor samples and 51 adjacent normal samples. Additionally, the GSE70768 dataset was obtained from the GEO database (https://www.ncbi.nlm.nih.gov/geo/), comprising 199 samples (125 tumor samples and 74 control samples) to enhance the statistical power of the study. During data analysis. tumor samples from TCGA-PRAD were stratified based on Gleason scores (GS) from clinical information. Using the internationally recognized Gleason grading system, samples were divided into five grades (Grade 1-5). Low-grade groups (Grade 1-3) corresponded to welldifferentiated tumors, while high-grade groups (Grade 4-5) indicated invasive biological behavior. This grading approach aligns with recent advancements in prostate cancer molecular mechanism research, where high Gleason grade tumors are often associated with key molecular events such as PTEN/AKT pathway alterations and changes in androgen receptor activity. The study design strictly adhered to public database usage guidelines, and data preprocessing involved the removal of duplicate and non-primary tumor samples to ensure reliability. For transcriptomic data normalization, TPM (Transcripts Per Million) conversion was applied to improve cross-sample comparability. This method is widely validated in TCGA data analyses.

Table 1. Real-time PCR primer information

Primer Name	Primer Sequence (5'-3')
RCBTB2-F	GGCTTGTGTCTTTGGCAGTG
RCBTB2-R	CCGAGGTTCAATGGTGCTCT
GPAA1-F	TAGTTGGAGGCGGGAGAGG
GPAA1-R	GTAGCTCAGCACGCACAAC
GAPDH-F	GTCTTCACCACCATGGAGAA
GAPDH-R	TAAGCAGTTGGTGGTGCAG

Quantification of RCBTB2 in the Human Protein Atlas (HPA) database

The HPA database (https://proteinatlas.org/) was utilized to query normal prostate tissue and PCa tissue samples. Well-preserved and properly stained IHC figures were selected to analyze the expression levels of RCBTB2 in PCa.

Cell culture

The human PCa cell line DU145 was acquired from OBiO Technology Corp., Itd. (Shanghai, China). DU145 cells were cultured in DMEM medium containing 10% FBS under conditions of 37°C and 5% $\rm CO_2$ in a humidified environment. All cell lines used in this study were maintained with a passage number not exceeding 20 generations.

Antibodies and plasmids

The antibodies used in this study included RCBTB2 Polyclonal antibody (13225-1-AP), GPAA1 Polyclonal antibody (10104-1-AP), N-cadherin Polyclonal antibody (22018-1-AP), E-cadherin Polyclonal antibody (20874-1-AP), Vimentin Polyclonal antibody (10366-1-AP), and GAPDH (10494-1-AP), all purchased from Proteintech (Wuhan, China). Goat Anti-rabbit IgG (A0208) and Goat Anti-mouse IgG (A0216) were got from Beyotime (Shanghai, China). The GL161 plasmid used in this study was obtained from OBiO Technology (Shanghai) Corp., Ltd. (Shanghai, China).

Construction of stable DU145 cell lines overexpressing RCBTB2 and with low GPAA1 expression

The lentiviruses LV-Ad-NC, LV-Ad-RCBTB2, LV-sh-NC, and LV-sh-GPAA1 were synthesized by OBiO Technology (Shanghai) Corp., Ltd. Lentiviral infection was conducted in accordance

with the manufacturer's guidelines. Cells were treated with puromycin (5 μ g/mL) for 2 weeks to establish stable monoclonal cell lines over-expressing RCBTB2 (DU145-OE) and with low GPAA1 expression (DU145-KD).

gRT-PCR

Total RNA was isolated utilizing the TRIzol kit (10606ES60, Yeasen Biotech, Shanghai, China). cDNA was synthesized following the instructions provided in the PrimeScript™ RT reagent Kit (RR047A, TAKARA, Japan). qRT-PCR was then conducted utilizing the Hieff® qPCR SYBR Green Master Mix (No Rox) kit (11202ES08, Yeasen Biotech, Shanghai, China). The relative expression levels of target genes were determined through the relative quantification method (2^{-∆∆Ct}). Primers were created utilizing the Primer-Blast online tool (**Table 1**).

Western blot

Total protein was isolated, and its concentration was determined with the Bradford Protein Assay Kit (AR0145, BOSTER, Wuhan, China). Equal amounts of protein (40 µg) from different samples were fractionated via 10% SDS-PAGE (SW109-01, Sevenbio, Beijing, China) and transferred onto PVDF membranes. The PVDF membranes were blocked with 5% non-fat milk and incubated overnight at 4°C with primary antibodies. Subsequently, the membranes were treated with HRP-conjugated secondary antibodies. Protein bands were detected using ECL detection reagent (BMU101-CN, Abbkine, Wuhan, China), and the band optical densities were evaluated using ImageJ software.

CCK-8

The Cell Counting Kit-8 (ATVMA0103, Abbkine, Wuhan, China) was employed to evaluate cell viability. Cells were seeded into a 96-well plate (2 \times 10 3 cells per well). After the cells adhered, at 0 h, 24 h, 48 h, and 72 h, 10 μL of CCK-8 reagent was introduced into each well for analysis. The plate was incubated at 37 $^{\circ}$ C for 3 h, and the OD value at 450 nm was assessed using a microplate reader.

Scratch assay

Cells were seeded into a 6-well plate containing 10% FBS medium and cultured for 24 h. When

the cell density reached 90-100%, a vertical scratch was made across the cell layer using a 10 μ L pipette tip, and the area was marked for identification. Detached cells were gently washed away with PBS, and the remaining cells were incubated in serum-free medium for another 24 h. Figures of the marked area were taken at 0 h and 24 h using an optical microscope.

Transwell assay

A total of 1×10^5 cells from each group were placed into the upper chamber of a Transwell coated with Matrigel, and medium containing 10% serum was added to the lower chamber. After incubation for 24 h, cells that traversed or penetrated the membrane were fixed using 4% paraformaldehyde. Unmigrated cells in the upper chamber were removed using cotton swabs. The migrated cells were stained with 0.1% crystal violet for 25 min, and figures were captured and counted under an inverted microscope.

Immunofluorescence staining

Processed cell slides were fixed with 4% paraformaldehyde, and then permeabilized with 0.1% Triton X-100 solution. Subsequently, the slides were blocked with 3% BSA at room temperature for 30 min. The slides were incubated overnight at 4°C with primary antibodies (dilution following the producer's guidelines), followed by incubation with corresponding fluorescently labeled secondary antibodies (dilution according to the manufacturer's instructions) at room temperature for 1 h. After DAPI nuclear staining, the slides were mounted and observed under a fluorescence microscope. Fluorescence intensity was semi-quantitatively analyzed using ImageJ software.

Nude mouse tumor formation assay

BALB/c-nude mice (male, 4-5 weeks old) were obtained from GemPharmatech Co., Ltd. (Nanjing, China). Mice were maintained under specific pathogen-free (SPF) conditions, with a 12-hour light/dark cycle, controlled temperature (22 \pm 1°C) and humidity (50 \pm 10%), and ad libitum access to food and water. DU145-OE and DU145-NC cells were subcutaneously injected into the mice at a dose of 2 \times 106 cells/100 µL per mouse (mice were divided into

two groups randomly, n = 6 for each group). During the cell injection process, mice were anesthetized with 2% isoflurane to relieve pain. Tumor formation and metastasis were analyzed by in vivo imaging on 24 d. After 8 weeks, the mice were euthanized, and tumor tissues were excised for histological analysis. Tumor morphology was observed using H&E staining. Euthanasia was performed by inhaling CO₂ (flow rate: 50% chamber volume per minute), followed by cervical dislocation. The animal experiment was approved by the Animal Care and Use Committee of Inner Mongolia People's Hospital (No. 202507204L; see Supplementary File). For the in vivo tumor imaging data, total photon flux (photons/second) within the region of interest (ROI) surrounding each tumor was quantified using the Living Image software.

H&E staining

The tissues were fixed in 4% paraformaldehyde solution, followed by routine dehydration and embedding. Paraffin sections with a thickness of $4~\mu m$ were prepared, stained, and mounted. Pathological morphological alterations in tumor tissues were examined using an optical microscope.

Co-immunoprecipitation

Cells were lysed on ice for 30 min in RIPA Lysis Buffer containing protease inhibitors (BL504A, Biosharp, Beijing, China). The lysates were centrifuged at 17,000 g for 30 min, and the supernatant was collected. A portion of 100 μL was reserved as the Input, while the remaining supernatant was incubated overnight at 4°C with Protein A/G magnetic beads and either a nonspecific antibody (Goat Anti-rabbit IgG, A0208, Beyotime, Shanghai, China) or a target-specific antibody. The beads were washed 3 times with lysis buffer and boiled for 5 min in 2 \times SDS loading buffer to elute the protein from the beads. Finally, the proteins in the IP samples were analyzed by Western blot.

Transcriptome sequencing and analysis

RNA was isolated from the DU145-NC and DU145-OE groups, and its quality was assessed. Poly-A-tailed mRNA was enriched using Oligo(dT)-coated magnetic beads. The mRNA was then fragmented, and the fragmented mRNA was used as a template for the synthesis

of first-strand cDNA. Subsequently, a secondstrand synthesis reaction system was prepared to generate double-stranded cDNA. The purified double-stranded cDNA underwent end repair and the addition of an "A" base at the 3' end. Sequencing adapters were then ligated to the cDNA. Approximately 200 bp cDNA fragments were selected, followed by PCR amplification. The constructed library underwent quality control through the Agilent 2100 Bioanalyzer, ensuring its suitability, before proceeding with sequencing. Gene expression levels for each sample were calculated, and the input data for differential gene expression analysis was derived from the reads count data obtained during gene expression analysis. Differential gene expression analysis was performed using edgeR software. The default criteria for significantly differentially expressed genes were set as P < 0.05 and $\lfloor \log FC \rfloor > 1$. The identified differentially expressed genes underwent GO functional annotation and KEGG pathway enrichment analysis.

Proteomics sequencing and analysis

Proteins were extracted from the DU145-NC and DU145-OE groups and subsequently digested into peptides. LC-MS/MS analysis was performed using the timsTOF Pro mass spectrometer (Bruker) combined with the Nanoelute system (Bruker Daltonics). Protein identification and quantitative analysis of raw mass spectrometry data were carried out using Max-Quant software. The default criteria for significantly differentially expressed proteins between samples were set as P < 0.05, with an upregulation threshold of FC > 2 or a downregulation threshold of FC < 0.5. Differentially expressed proteins were further analyzed through clustering, subcellular localization, domain analysis, GO functional annotation, and KEGG pathway enrichment analysis.

Ubiquitination proteomics sequencing and analysis

Proteins were extracted from the DU145-NC and DU145-OE groups, digested into peptides, and further enriched for ubiquitinated peptides. LC-MS/MS analysis was conducted using the timsTOF Pro mass spectrometer (Bruker) in combination with the Nanoelute system (Bruker Daltonics). Protein modification identification and quantitative analysis of raw mass

spectrometry data were performed using MaxQuant software. The default criteria for significant differentially modified peptides between samples were set as P < 0.05, with an upregulation threshold of FC > 2 or a downregulation threshold of FC < 0.5. Subsequently, the differentially modified peptides underwent clustering analysis, conserved motif analysis, subcellular localization analysis, domain analysis, GO functional annotation, and KEGG pathway enrichment analysis.

Statistical analysis

All statistical results are expressed as mean ± SD based on three independent biological replicates. For the in vivo tumor imaging data, each group consisted of six mice (n = 6)Statistical analyses were performed using a 2-tailed unpaired Student's t-test for comparisons between two groups, or Repeated Measures ANOVA followed by Tukey's post hoc test for continuous time point data. All figures and statistical analyses were generated using GraphPad Prism 8.0. P < 0.05 was considered to be statistically significant (*P < 0.05, **P <0.01, ***P < 0.001, ****P < 0.0001). Appropriate statistical tests were selected and justified for each figure based on the experimental design and data distribution.

Results

RCBTB2 is a negative regulatory gene in PCa progression

Transcriptome analysis data and corresponding clinical information of PCa were downloaded from the TCGA database, totaling 483 tumor samples and 51 control samples. Based on clinical data. Gleason scores in TCGA-PRAD were classified into 5 grades (1-5). Additionally, transcriptomic data from GSE70768, consisting of 125 tumor samples and 747 control samples, were downloaded from the GEO database. Pearson correlation analysis was performed on the FPKM_UQ values of each gene from the TCGA transcriptomic data and Gleason group grades. Results indicated that the gene most negatively correlated with Gleason groups was RCBTB2. Visualization was conducted for the top five negatively correlated genes - RCBTB2, SRD5A2, FAM107A, CDC42E-P4, and PPARGC1A (Figure 1A, 1B). Further investigation using transcriptomic data from

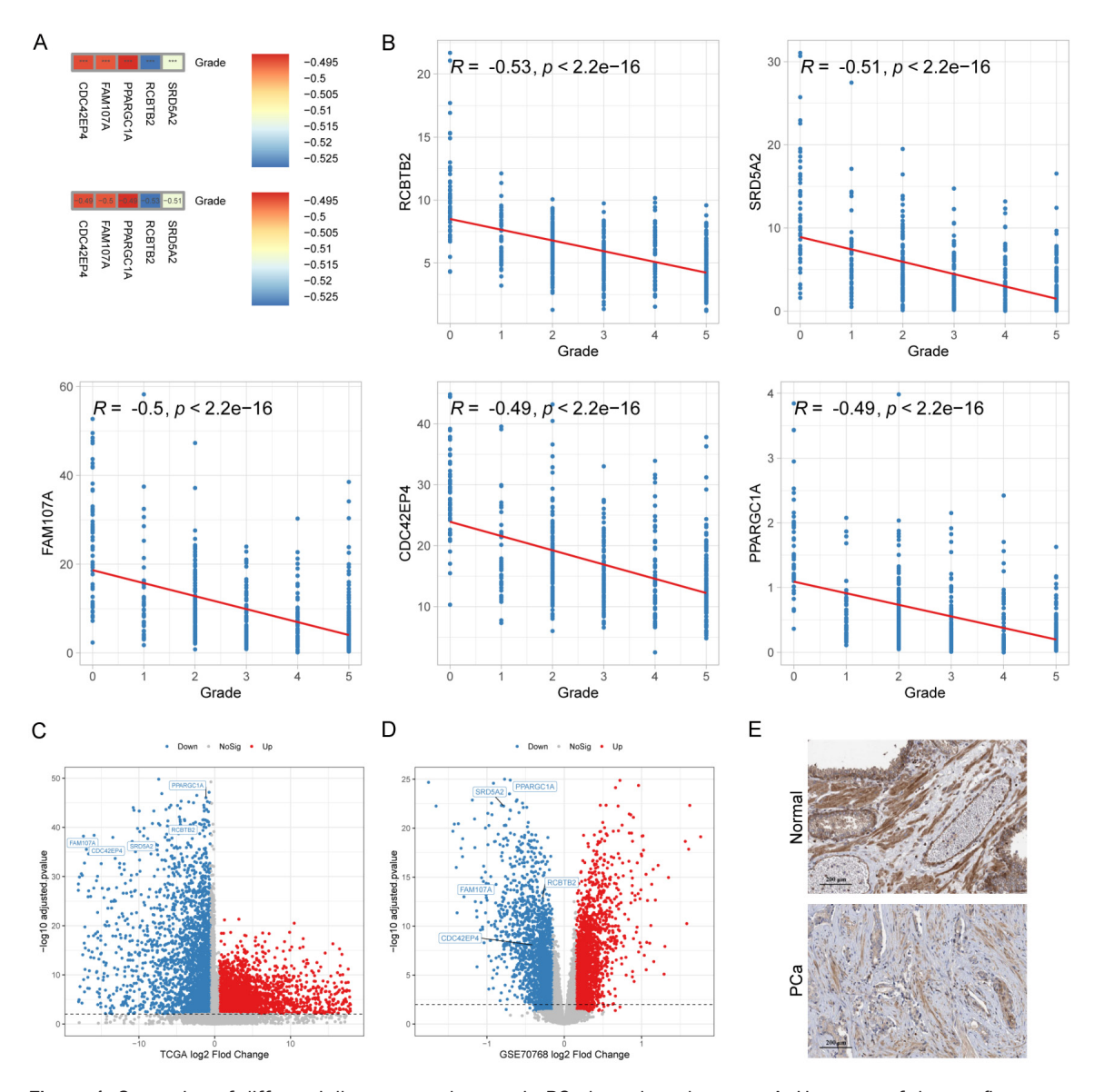


Figure 1. Screening of differentially expressed genes in PCa based on datasets. A. Heatmap of the top five genes negatively correlated with Gleason group grades. B. Visualization of correlations between the FPKM_UQ values of RCBTB2, SRD5A2, FAM107A, CDC42EP4, and PPARGC1A with Gleason group grades. C. Volcano plot of differential gene expression distribution in the TCGA-PRAD dataset. D. Volcano plot of differential gene expression distribution in the GSE70768 transcriptomic dataset. E. Analysis of RCBTB2 expression levels in prostate tissues based on the HPA dataset. Images were captured at 100× magnification.

TCGA-PRAD and GSE70768 revealed that these genes were significantly downregulated in tumor samples compared to controls (Figure 1C, 1D). Excluding the other 4 genes, RCBTB2 showed the strongest correlation with PCa and was the most likely tumor suppressor gene. Pathological images of PCa patients from the HPA database were analyzed to compare the expression levels of RCBTB2 between normal prostate tissues and PCa tissues. Outcomes indicated that the expression level of RCBTB2 was significantly lower in the PCa group com-

pared to the normal group (**Figure 1E**). Thus, RCBTB2 will be further studied to explore its molecular mechanisms (and its target proteins) in affecting PCa progression.

In vitro cell experiments show overexpression of RCBTB2 weakens malignant biological behavior in PCa cells

To investigate the biological function of RCBT-B2 in PCa, DU145 cells with low endogenous RCBTB2 expression were selected as the

experimental model, and a monoclonal cell line stably overexpressing RCBTB2 (DU145-OE) was established. First, quantitative analysis of RCBTB2 mRNA and protein expression levels in DU145 cells was performed using gRT-PCR and Western blot. The results showed that RCBTB2 mRNA and protein expression levels were significantly higher in DU145-OE cells than in DU145-NC cells (Figure 2A, 2B). Next, CCK-8 cell proliferation assays were conducted on both groups of cells. The results indicated that the proliferation activity of DU145-OE cells was significantly weakened compared to DU145-NC cells (Figure 2C). In PCa, EMT is a key process leading to late-stage metastasis. To confirm whether RCBTB2 mediates the EMT pathway, immunofluorescence staining was performed to analyze the expression of E-cadherin, N-cadherin, and Vimentin in the cells. The findings revealed a notable elevation in E-cadherin fluorescence intensity within DU145-OE cells, while N-cadherin and Vimentin fluorescence intensities were noticeably decreased compared to DU145-NC cells (Figure 2D). This suggests that overexpression of RCBTB2 reverses EMT progression in PCa cells. To assess the impact of RCBTB2 on cell migration and invasion capabilities, scratch assays and Transwell assays were performed. The results revealed that DU145-OE cells exhibited significantly reduced migration and invasion abilities compared to DU145-NC cells (Figure 2E, 2F). In summary, these findings indicated that RCBTB2 can inhibit the malignant biological behavior of prostate cancer cells in vitro.

In vivo animal experiments show overexpression of RCBTB2 suppresses tumor formation in nude mice

To gain deeper insights into the role of RCBTB2 in PCa, a subcutaneous xenograft tumor model was established using severely immunodeficient mice. Experimental results indicated that DU145-NC group mice developed noticeable primary tumors and partial metastatic lesions after inoculation, while overexpression of RCBTB2 significantly inhibited tumor formation and progression (Figure 3A). HE staining results revealed that the tumor tissues from the DU145-NC group had abundant cells, irregular and dense arrangements, with prominent tumor cell atypia and evidence of nuclear division (black arrows). Within these tissues, inflammatory cells were observed infiltrating in

bands (yellow arrows), with no evident necrotic lesions. The tumor tissues from the DU145-OE group showed prominent cell atypia with signs of nuclear division (black arrows), a reduction in cell numbers, notable apoptosis, structural damage, and localized necrosis within the tumor tissue (red arrows) (Figure 3B). These findings suggest that RCBTB2 may exert its tumor-suppressive effects through mechanisms involving tumor microenvironment regulation, which requires further elucidation.

Identification of downstream regulatory genes of RCBTB2

Bulk RNA-seq analysis was performed on DU145-NC and DU145-OE stable cell lines to explore the effects of RCBTB2 overexpression on gene expression in DU145 cells. The outcomes demonstrated that, in comparison to the DU145-NC group, 482 genes, including CXCL1 and CXCL8, were significantly upregulated, while 586 genes, such as MUC1 and PLPP3, were significantly downregulated. Additionally, 30,478 genes, including GPAA1 and LAMB3, showed no significant changes in expression (Figure 4A). Further investigation using GSEA enrichment analysis identified the top five significant pathways based on the absolute value of the normalized enrichment score (NES). These pathways included Regulation of Autophagy, Cytokine-Cytokine Receptor Interaction, NOD-Like Receptor Signaling Pathway, Prion Diseases, and Folate Biosynthesis, which were found to have important biological significance (Figure 4B).

Identification of downstream regulatory proteins of RCBTB2

4D Label-free proteomics analysis was conducted on DU145-NC and DU145-OE stable cell lines to investigate the effects of RCBTB2 overexpression on protein expression levels in DU145 cells by identifying differences in protein expression between the RCBTB2-over-expressing group and the control group. Compared to the DU145-NC group, 8 proteins, including O43402 and B1ANY6, were significantly upregulated in the DU145-OE group, while 21 proteins, such as A0A994J3Z2 (GPAA1) and O14841, were significantly down-regulated (Figure 5A, 5B). Notably, GPAA1 transcriptomic expression did not exhibit significant changes under RCBTB2 overexpres-

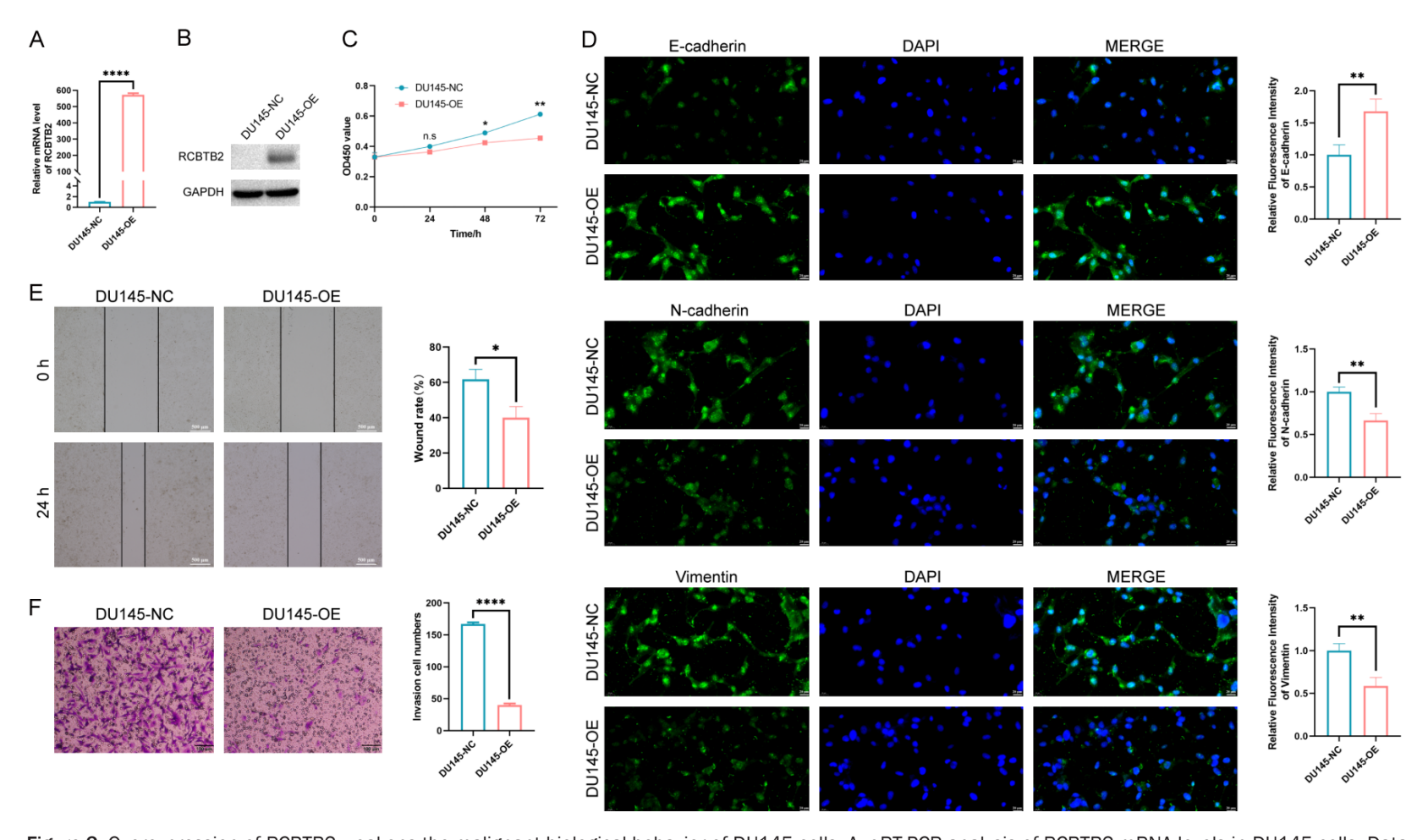


Figure 2. Overexpression of RCBTB2 weakens the malignant biological behavior of DU145 cells. A. qRT-PCR analysis of RCBTB2 mRNA levels in DU145 cells. Data are shown as mean \pm SD of 3 independent experiments. ****P < 0.0001, t-test. B. Western blot analysis of RCBTB2 protein levels in DU145 cells. C. CCK-8 assay to assess DU145 cell proliferation. Data are shown as mean \pm SD of 3 independent experiments. n.s, no significance, **P < 0.01, ***P < 0.001, Repeated Measures ANOVA followed by Tukey's post hoc test. D. Immunofluorescence staining to detect the expression of E-cadherin, N-cadherin, and Vimentin in DU145 cells. Right: Semi-quantitative analysis of fluorescence intensity. Images were captured at 400× magnification. Data are shown as mean \pm SD of 3 independent experiments. **P < 0.01, t-test. E. Scratch assay to evaluate DU145 cell migration ability. Images were captured at 100× magnification. Data are shown as mean \pm SD of 3 independent experiments. *P < 0.05, t-test. F. Transwell assay to assess DU145 cell invasion ability. Images were captured at 100× magnification. Data are shown as mean \pm SD of 3 independent experiments. ***P < 0.0001, t-test.

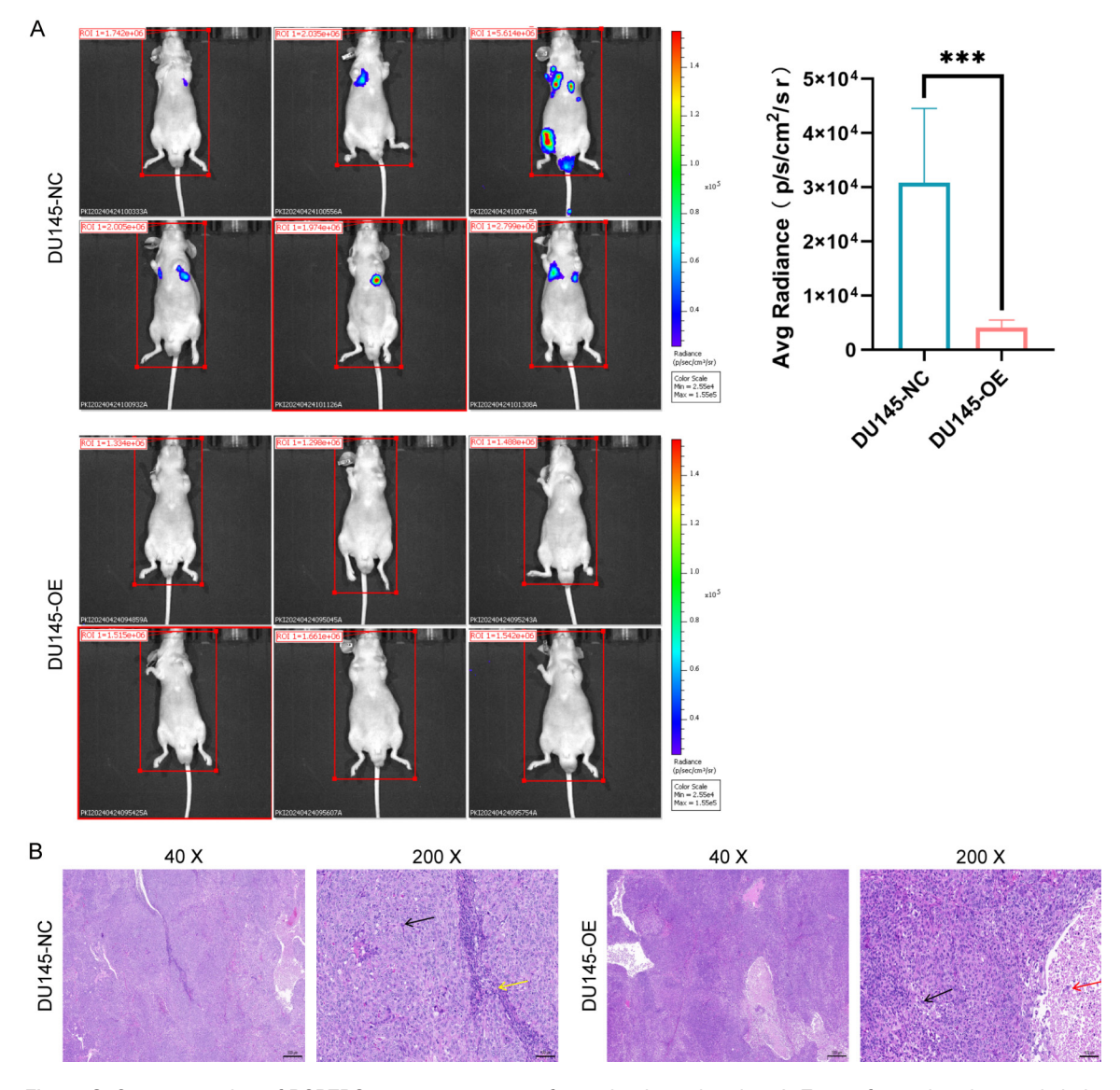


Figure 3. Overexpression of RCBTB2 suppresses tumor formation in nude mice. A. Tumor formation detected via in vivo imaging on 24d post-cell inoculation (n = 6). Right: Quantitative analysis of tumor fluorescence intensity. Data are shown as mean \pm SD of 6 independent experiments. ***P < 0.001, t-test. B. HE staining to observe pathological morphological changes in tumor tissues. Images were captured at 40× and 200× magnification.

sion. To gain a thorough understanding of the functions, localization, and biological pathways associated with these proteins, GO and KEGG enrichment analyses were performed to annotate and analyze them. The results revealed that these significantly different proteins are involved in tumor immunity-related pathways such as the IL-17 signaling pathway and Th1 and Th2 cell differentiation (Figure 5C).

GPAA1 might be a target gene regulated by RCBTB2 in PCa

A systematic analysis was conducted on DU145-NC and DU145-OE stable cell lines

using 4D Label-free ubiquitination proteomics technology to uncover the regulatory effects of RCBTB2 overexpression on protein ubiquitination levels. A total of 2,392 ubiquitinated proteins, 6,412 ubiquitinated peptides, and 7,387 ubiquitination sites were identified. After strict quantitative screening, 2,389 quantifiable ubiquitinated proteins (covering 6,398 quantifiable peptides) and 7,371 quantifiable ubiquitination sites were obtained (**Figure 6A**). To analyze the distribution characteristics of ubiquitination modification sites on proteins, the number of ubiquitination sites on all identified proteins was statistically calculated. The results

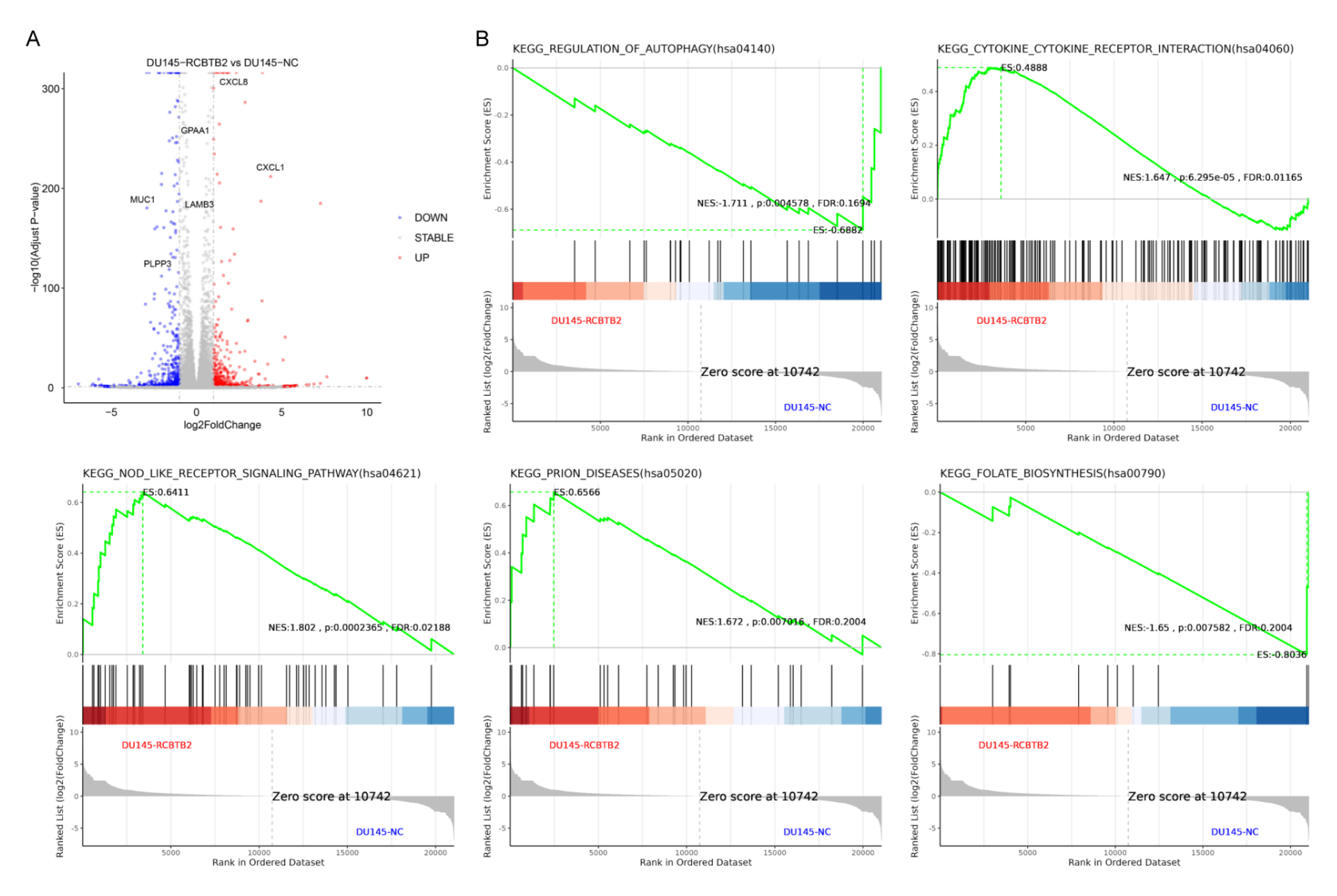


Figure 4. Bulk RNA-seq Analysis of DU145-NC and DU145-OE. A. Volcano plot depicting the distribution of differentially expressed genes. B. Illustration of the GSEA enrichment analysis results.

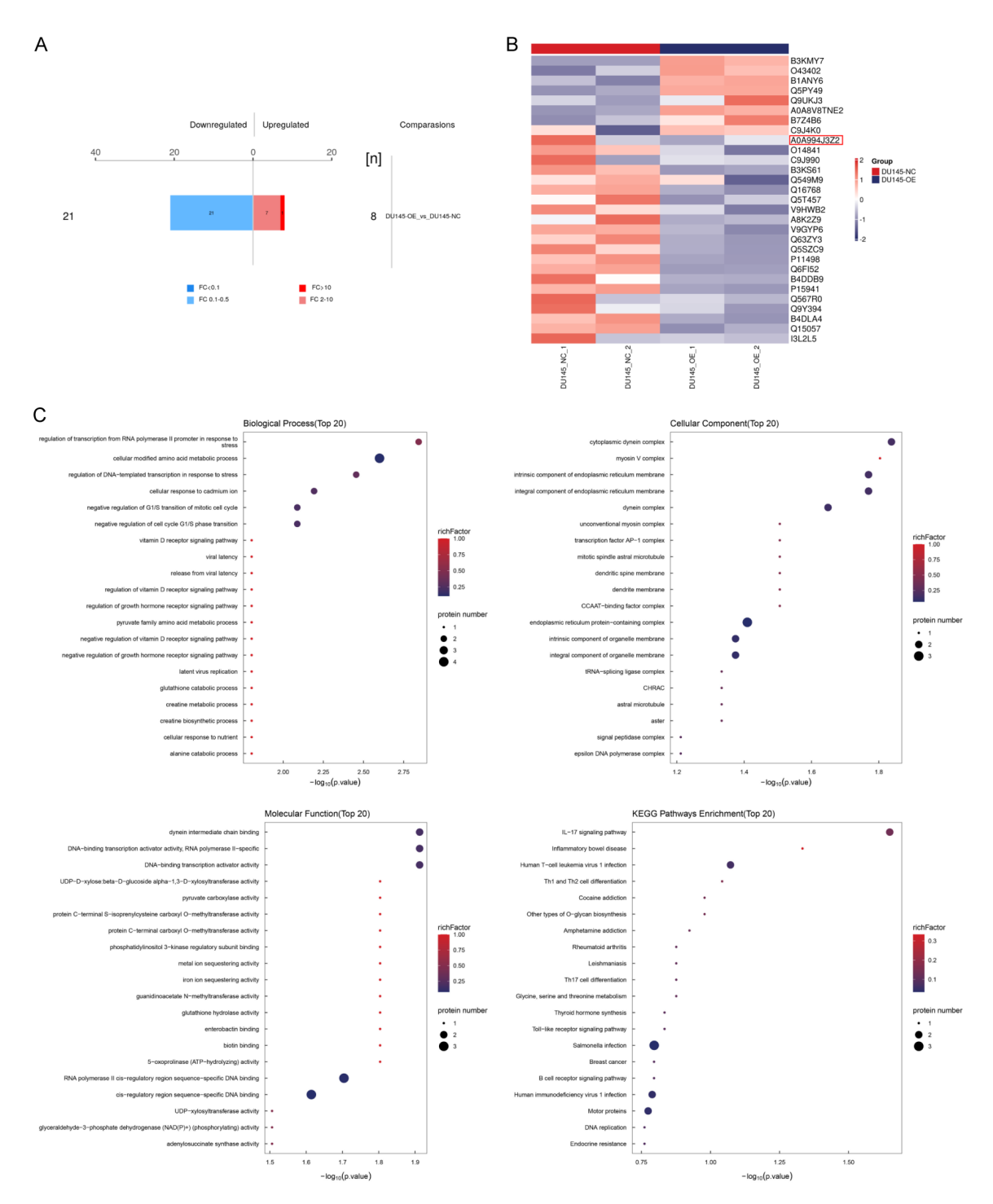


Figure 5. 4D label-free proteomics analysis of DU145-NC and DU145-OE. A. Bar chart showing quantitative differences in protein expression. B. Heatmap of clustering analysis for differentially expressed proteins. C. Bubble chart of GO/KEGG enrichment analysis for differentially expressed proteins.

showed that 52.38% of proteins contained two or more ubiquitination sites, with protein Q09666 exhibiting up to 190 ubiquitination sites (**Figure 6B**). Quantitative analysis of ubiquitination modification sites showed that, on

average, all identified modified proteins contained 24.27 ubiquitination modification sites per 100 amino acids (Figure 6C). To further evaluate the overlap characteristics of ubiquitination modifications between different experi-

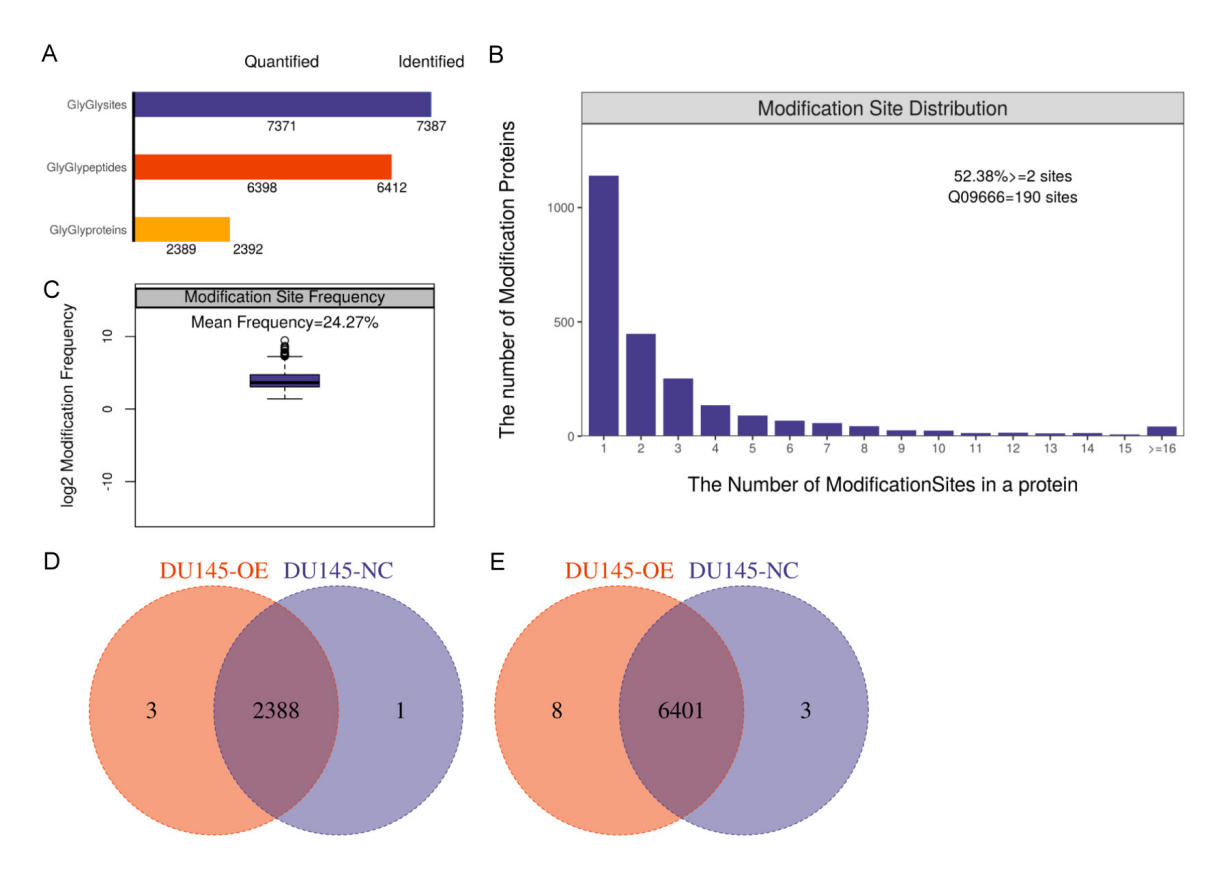


Figure 6. Ubiquitination Proteomics Analysis of DU145-NC and DU145-OE. A. Bar chart of identification and quantification results. B. Distribution chart of the number of ubiquitination modification sites. C. Frequency distribution chart of ubiquitination modification sites. D. Venn diagram of ubiquitinated proteins identified between groups. E. Venn diagram of ubiquitinated peptides identified between groups.

mental groups, a Venn diagram was used for visualization. The results revealed 2,388 overlapping ubiquitinated proteins and 6,401 overlapping ubiquitinated peptides among the groups (Figure 6D, 6E). Additionally, by crossreferencing transcriptomic and proteomic data, transcriptional regulatory interference was excluded, allowing for the precise identification of RCBTB2-specific substrates, where mRNA stability was maintained, but proteins underwent significant degradation-namely, GPAA1. The ubiquitination level of the GPAA1 protein was further investigated. Results showed an upward trend in GPAA1 ubiquitination levels in the DU145-OE group compared to the DU145-NC group, though this difference was not statistically significant, potentially due to the limited sample size.

By integrating the results of Bulk RNA-seq, 4D Label-free proteomics, and 4D Label-free ubiquitination proteomics analyses, it was observed that RCBTB2 overexpression did not affect

GPAA1 at the transcriptional level. However, significant downregulation was detected at the protein level, alongside an increase in GPAA1 ubiquitination levels. This suggests that RCBTB2 may regulate PCa progression through its interaction with GPAA1. Hence, subsequent studies will focus on investigating the specific mechanisms by which RCBTB2 targets and regulates GPAA1, as well as its specific roles and functions in PCa.

Validation of the interaction between RCBTB2 and GPAA1

Previous multi-omics analysis results suggested a functional correlation between GPAA1 and RCBTB2. To confirm this hypothesis, immuno-fluorescence techniques were used to analyze the cellular colocalization of RCBTB2 and GPAA1 proteins in the DU145-OE cell line. Experimental results showed that overexpression of RCBTB2 led to a significant increase in the fluorescence intensity of RCBTB2 protein,

while the fluorescence intensity of GPAA1 protein was significantly reduced. Additionally, RCBTB2 and GPAA1 proteins exhibited colocalization in subcellular structures, suggesting the possibility of a protein-protein interaction between them (Figure 7A). To further confirm the interaction between RCBTB2 and GPAA1, Co-IP experiments were conducted in DU145-OE cell lines, and the results verified that GPAA1 is an interacting protein of RCBTB2 (Figure 7B).

GPAA1 may influence malignant biological behavior of PCa cells through autophagy aggregate mediation

To explore the functional role of GPAA1 in PCa. stable cell lines with low GPAA1 expression (DU145-KD) were successfully established using lentivirus-mediated shRNA interference technology, with DU145-NC serving as the control group. First, gRT-PCR and Western blot were used to validate the mRNA and protein expression levels of GPAA1 in DU145 cells. The experimental results showed that, compared to the DU145-NC group, the DU145-KD group exhibited a significant reduction in both mRNA and protein expression levels of GPAA1 (Figure 8A, 8B). Subsequently, CCK-8 assays were performed to evaluate the proliferative activity of both groups of cells. The results demonstrated that the DU145-KD group exhibited significantly reduced proliferation activity compared to the DU145-NC group (Figure 8C). To further assess the impact of GPAA1 on cell migration and invasion abilities, scratch assays and Transwell experiments were conducted. The results revealed that the migration and invasion abilities of DU145-KD cells were significantly reduced compared to DU145-NC cells (Figure 8D, 8E). Following this, immunofluorescence staining was employed to examine the cellular expression levels of E-cadherin, N-cadherin, and Vimentin. The results showed that in DU145-KD cells, the fluorescence intensity of E-cadherin was significantly enhanced, while the fluorescence intensities of N-cadherin and Vimentin were notably reduced (Figure 8F, left). This indicates that knocking down GPAA1 can effectively reverse the EMT process in PCa cells. These findings indicate that GPAA1 can suppress the malignant biological behavior of prostate cancer cells in vitro. Furthermore, the fluorescence intensities of autophagy-related

factors p62, NBR1, and CCT2 were significantly reduced (**Figure 8F**, right), suggesting that GPAA1 may influence the malignant phenotype of PCa cells by regulating the degradation process of protein aggregates. The reduced expression of p62, NBR1, and CCT2 - established markers of aggrephagy - suggests a potential association with aggrephagy in the malignant phenotype of PCa cells. However, confirmation requires further investigation using aggrephagy-specific assays, such as p62-LC3 co-immunoprecipitation.

Discussion

This study was the first to reveal the molecular mechanism by which the E3 ubiquitin ligase RCBTB2 inhibited the malignant progression of PCa through ubiquitination-mediated degradation of GPAA1. Low expression of RCBTB2 in PCa was significantly correlated with higher tumor malignancy, whereas overexpression of RCBTB2 suppressed cancer cell proliferation, migration, invasion, and the EMT process by promoting ubiquitin-dependent degradation of GPAA1. This discovery not only expanded the understanding of the ubiquitination regulatory network in PCa but also provided new directions for therapeutic strategies targeting protein homeostasis.

As an E3 ubiquitin ligase, the function of RCBTB2 relies on its specific recognition and ubiquitination of substrate proteins. By integrating transcriptomic, proteomic, and ubiquitinomic data, it was found that the protein level of GPAA1 significantly decreased upon RCBTB2 overexpression, while its mRNA level remained unaffected. This suggested that RCBTB2 regulates GPAA1 stability through post-translational modification. Ubiquitin proteomics further revealed an increase in GPAA1 ubiquitination levels, and Co-IP confirmed the direct interaction between RCBTB2 and GPAA1. This indicated that RCBTB2 likely mediate the ubiquitination and degradation of GPAA1 as an E3 ubiquitin ligase. This discovery, for the first time, established a link between RCBTB2 and the metabolism of GPI-anchored proteins, expanding the known substrate spectrum of RCBTB2.

The role of the ubiquitination system in tumors has been extensively studied, and RCBTB2 has been suggested as a potential tumor suppressor gene in cancers such as lymphoblastic leu-

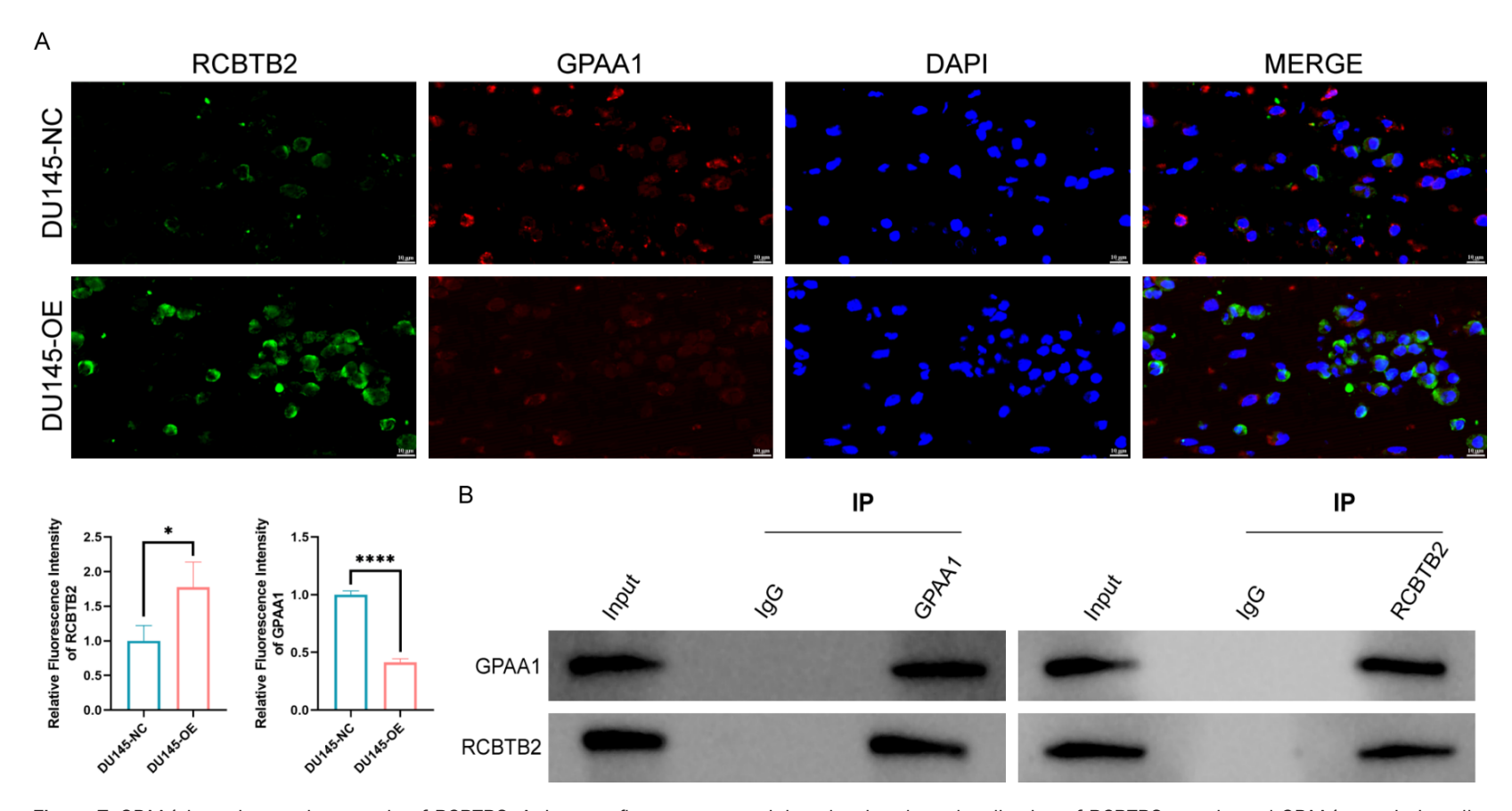
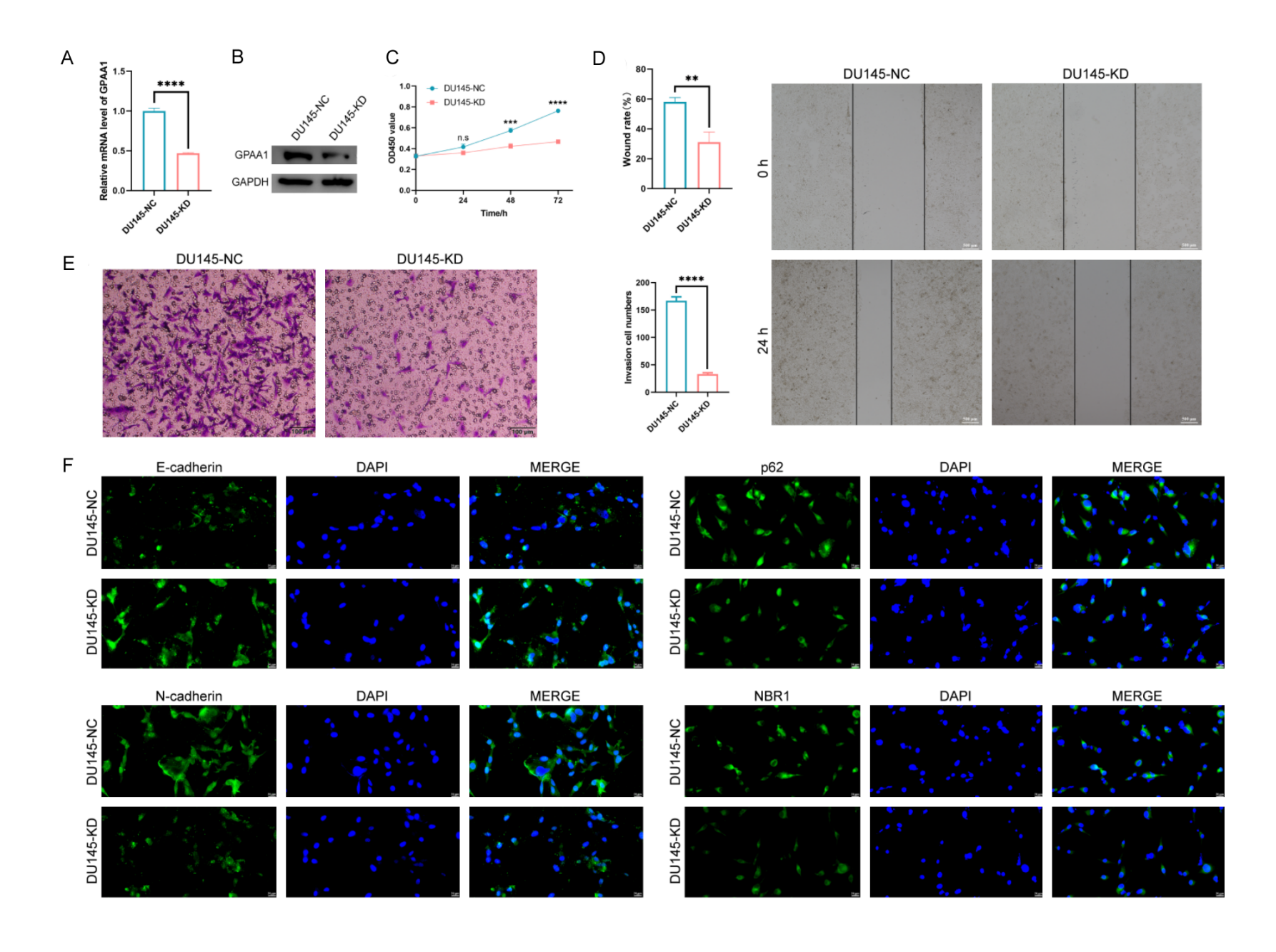


Figure 7. GPAA1 is an interacting protein of RCBTB2. A. Immunofluorescence staining showing the colocalization of RCBTB2 protein and GPAA1 protein in cells. Below: Semi-quantitative analysis of fluorescence intensity. Images were captured at 1000× magnification. Data are shown as mean ± SD of 3 independent experiments. *P < 0.05, ****P < 0.001, t-test. B. Co-IP analysis demonstrating the interaction between RCBTB2 protein and GPAA1 protein.



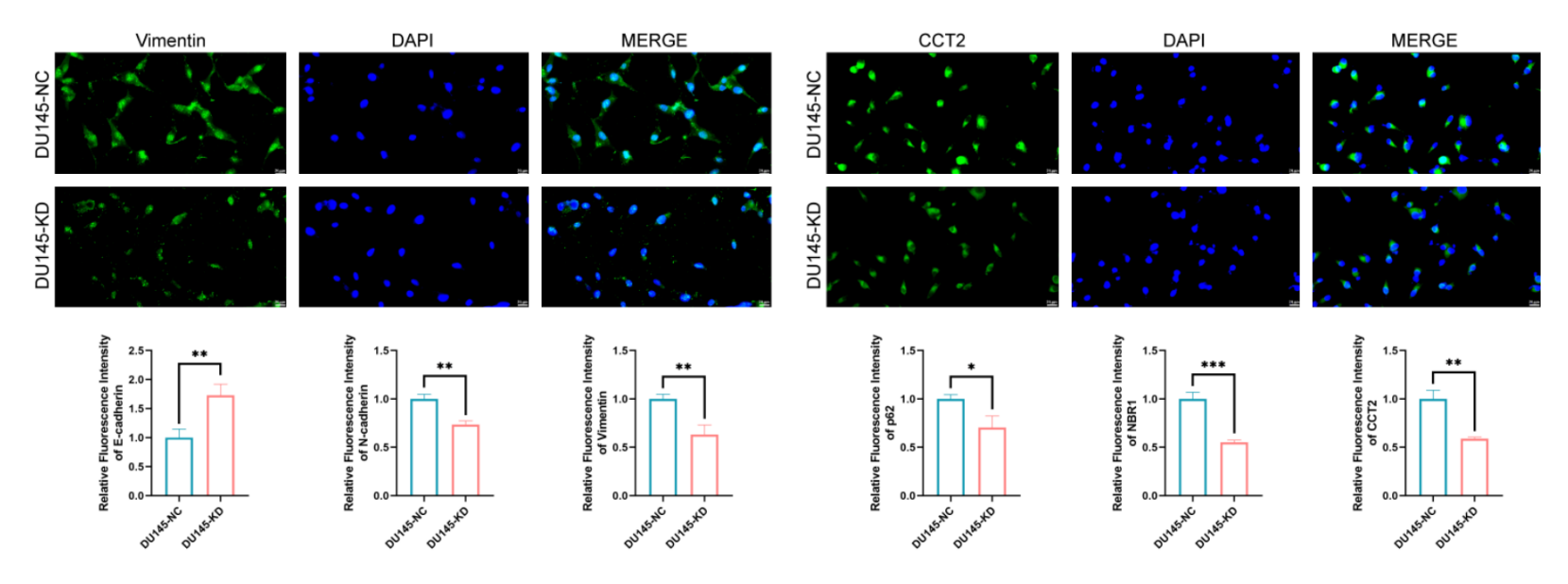


Figure 8. Reduced GPAA1 Expression Weakens the Malignant Biological Behavior of DU145 Cells. A. qRT-PCR analysis of GPAA1 mRNA levels in DU145 cells. Data are shown as mean \pm SD of 3 independent experiments. ****P < 0.0001, t-test. B. WB analysis of GPAA1 protein levels in DU145 cells. C. CCK-8 assay evaluating the proliferative capacity of DU145 cells. Data are shown as mean \pm SD of 3 independent experiments. n.s, no significance, ***P < 0.001, ****P < 0.0001, Repeated Measures ANOVA followed by Tukey's post hoc test. D. Scratch assay assessing the migration ability of DU145 cells. Images were captured at 100× magnification. Data are shown as mean \pm SD of 3 independent experiments. **P < 0.05, t-test. E. Transwell assay analyzing the invasion ability of DU145 cells. Images were captured at 100× magnification. Data are shown as mean \pm SD of 3 independent experiments. ****P < 0.0001, t-test. F. Immunofluorescence staining showing the expression of E-cadherin, N-cadherin, and Vimentin (left), and autophagy-related factors p62, NBR1, and CCT2 (right) in DU145 cells. Below: Semi-quantitative analysis of fluorescence intensity. Images were captured at 400× magnification. Data are shown as mean \pm SD of 3 independent experiments. *P < 0.05, **P < 0.01, ***P < 0.001, t-test.

kemia, lung adenocarcinoma, and colorectal cancer, although its specific mechanism of action remains unclear [17-19]. Moreover, the function of RCBTB2 and its substrates in PCa have not been elucidated. This study was the first to establish a connection between RCBTB2 and GPAA1, uncovering its unique mechanism of regulating PCa via the ubiquitination-proteasome pathway. Additionally, GPAA1 is abnormally overexpressed in various tumors, but reports on its upstream regulatory factors are scarce. These findings bridged this gap and suggested that the RCBTB2-GPAA1 axis may exhibit tissue-specific regulatory characteristics.

GPAA1 serves as a critical subunit of glycosylphosphatidylinositol (GPI) transamidase and directly contributes to tumor initiation and progression through anchoring related proteins [20-22]. In ovarian cancer, GPAA1 promotes GPI anchoring of CD24. Once the expression of CD24 on the cell surface increases, macrophage-mediated phagocytosis is weakened, thereby facilitating ovarian tumor growth. Targeting GPAA1 could be a potential immunotherapeutic strategy for CD24-positive ovarian cancer [23]. In gastric cancer, GPAA1 expression is independently related to poor survival and prognosis in patients. Furthermore, GPAA1 regulated the interaction between EGFR and ERBB2, stimulating downstream signaling pathways to promote tumor growth [24]. However, the relationship between GPAA1 and PCa had not yet been clarified. In this study, it was found that GPAA1 knockdown not only inhibited PCa cell proliferation, migration, invasion, and EMT processes but also regulated the expression of aggrephagy-related factors such as p62 and NBR1. This suggested that GPAA1 might have promoted tumor progression by modulating aggrephag pathways. Although p62 and NBR1 are recognized aggrephagy markers, definitive evidence requires dedicated assays such as LC3 flux analysis or ubiquitinated protein clearance measurements. Aggrephagy was an important process that cleared misfolded proteins to maintain cell health. When it was abnormally activated, it was often linked to the progression of tumors [25-27]. This finding provided a novel perspective on the cross-mechanism between GPI-anchored protein metabolism and autophagy regulation in PCa.

We acknowledge that rescue experiments would provide stronger evidence for a causal relationship between RCBTB2 and GPAA1, and that validation across additional PCa cell lines (e.g., LNCaP, PC3) would enhance the generalizability of our findings. However, due to resource constraints, these experiments were not feasible in the current study. Despite this, our cumulative data support GPAA1 as a downstream effector of RCBTB2. This is evidenced by phenotypic parallels between RCBTB2 overexpression and GPAA1 knockdown - both suppressing PCa cell proliferation, migration, and epithelial - mesenchymal transition (EMT; Figures 2, 8) - as well as their direct interaction (Figure 7) and increased GPAA1 ubiquitination in RCBTB2-overexpressing cells (Figure 6), collectively suggesting a functional axis. Furthermore, DU145 cells represent a well-established model of castration-resistant prostate cancer (CRPC), and consistent RCBTB2 downregulation across diverse PCa datasets (TCGA/GEO; Figure 1) supports the broader relevance of our findings. Future studies incorporating rescue experiments and additional cell lines or xenograft models are planned to further substantiate this axis.

Although this study systematically analyzed the molecular mechanism of the RCBTB2-GPAA1 axis, there were several limitations. Firstly, due to resource constraints, we have not yet performed rescue experiments (e.g., co-expression of RCBTB2 and GPAA1) to further confirm the causal relationship between the RCBTB2-GPAA1 axis and PCa malignant phenotypes. Secondly, functional assays were only conducted in DU145 cells, and validation in additional PCa cell lines (e.g., LNCaP, PC3) to enhance the generalizability of findings was not feasible in the current study. Thirdly, the observed increase in GPAA1 ubiquitination levels in the ubiquitin proteomics analysis did not reach statistical significance, which may be attributed to limitations in sample size or technical sensitivity, requiring more rigorous validation in future studies. Fourthly, direct evidence demonstrating that RCBTB2 mediates GPAA1 ubiquitination (e.g., in vitro ubiquitination assays using purified RCBTB2 and GPAA1 proteins) is still lacking, which is essential to confirm their direct regulatory relationship. Fifthly, the specific ubiquitination sites of GPAA1 targeted by RCBTB2 were not clearly identified, requiring further validation through

mass spectrometry or site-directed mutagenesis experiments. Sixthly, whether RCBTB2 has functional redundancy with other E3 ubiquitin ligases or deubiquitinases remains to be explored in broader models. Finally, the mechanism by which GPAA1 regulates aggrephagy remains unclear - while reduced expression of aggrephagy markers (p62, NBR1, CCT2) was observed in GPAA1-knockdown cells (Figure 8F), how GPAA1 specifically modulates this process (e.g., via interacting with autophagy-related proteins) and whether it reshapes the tumor microenvironment by influencing misfolded protein clearance still requires in-depth investigation.

Thus, future research will aim to delve into the interaction domains between RCBTB2 and GPAA1, clarifying the ubiquitination modification sites. Additionally, developing small-molecule agonists targeting RCBTB2 or GPAA1 degraders and evaluating their synergistic efficacy in combination with immune checkpoint inhibitors could provide promising therapeutic strategies. Moreover, the mechanism by which GPAA1 regulates aggrephagy requires further clarification, particularly regarding whether it reshapes the tumor microenvironment by influencing the clearance of misfolded proteins. Future studies will prioritize addressing these limitations - including conducting rescue experiments, expanding validation to multiple PCa cell lines, performing in vitro ubiquitination assays to confirm direct regulation, identifying specific ubiquitination sites of GPAA1, and clarifying how GPAA1 modulates aggrephagy to further validate and extend the current findings on the RCBTB2-GPAA1 axis.

In summary, this study elucidated the molecular mechanism by which RCBTB2 inhibits PCa progression through the ubiquitination of GPAA1, providing a theoretical foundation for therapies targeting protein homeostasis. The identification of the RCBTB2-GPAA1 axis not only deepened the understanding of PCa pathogenesis but also laid the scientific groundwork for developing novel combination therapies. Future research should further investigate its clinical translational potential, aiming to offer more precise therapeutic strategies for PCa patients.

Acknowledgements

This research was funded by The National Natural Science Foundation of China (No. 817-

60463), Natural Science Found of Inner Mongolia (2023MS08015) and Central Government Funds for Guiding Local Scientific and Technological Development (No. 2021ZY0037).

Disclosure of conflict of interest

None.

Address correspondence to: Sanxiang Li and Chunxiao Liu, Department of Urology, Zhujiang Hospital, Southern Medical University, No. 253, Middle Industrial Avenue, Haizhu District, Guangzhou 510280, Guangdong, China. E-mail: 13947-149991@163.com (SXL); liuchx888@163.com (CXL)

References

- [1] Bergengren O, Pekala KR, Matsoukas K, Fainberg J, Mungovan SF, Bratt O, Bray F, Brawley O, Luckenbaugh AN, Mucci L, Morgan TM and Carlsson SV. 2022 update on prostate cancer epidemiology and risk factors-a systematic review. Eur Urol 2023; 84: 191-206.
- [2] Hansen SB, Unal B, Kuzu OF and Saatcioglu F. Immunological facets of prostate cancer and the potential of immune checkpoint inhibition in disease management. Theranostics 2024; 14: 6913-6934.
- [3] Zhang D and Tang DG. "Splice" a way towards neuroendocrine prostate cancer. EBioMedicine 2018; 35: 12-13.
- [4] Van Veldhuizen PJ. Prostate cancer active surveillance: quality matters. J Natl Compr Canc Netw 2023; 21: 529-530.
- [5] Hawley JE, Obradovic AZ, Dallos MC, Lim EA, Runcie K, Ager CR, McKiernan J, Anderson CB, Decastro GJ, Weintraub J, Virk R, Lowy I, Hu J, Chaimowitz MG, Guo XV, Zhang Y, Haffner MC, Worley J, Stein MN, Califano A and Drake CG. Anti-PD-1 immunotherapy with androgen deprivation therapy induces robust immune infiltration in metastatic castration-sensitive prostate cancer. Cancer Cell 2023; 41: 1972-1988, e1975.
- [6] Dai C, Dehm SM and Sharifi N. Targeting the androgen signaling axis in prostate cancer. J Clin Oncol 2023; 41: 4267-4278.
- [7] Nag S, Goswami B, Das Mandal S and Ray PS. Cooperation and competition by RNA-binding proteins in cancer. Semin Cancer Biol 2022; 86: 286-297.
- [8] Yedla P, Babalghith AO, Andra VV and Syed R. PROTACs in the management of prostate cancer. Molecules 2023; 28: 3698.
- [9] Liu F, Chen J, Li K, Li H, Zhu Y, Zhai Y, Lu B, Fan Y, Liu Z, Chen X, Jia X, Dong Z and Liu K. Ubiquitination and deubiquitination in cancer: from mechanisms to novel therapeutic approaches. Mol Cancer 2024; 23: 148.

- [10] Kuang Z, Liu X, Zhang N, Dong J, Sun C, Yin M, Wang Y, Liu L, Xiao D, Zhou X, Feng Y, Song D and Deng H. USP2 promotes tumor immune evasion via deubiquitination and stabilization of PD-L1. Cell Death Differ 2023; 30: 2249-2264.
- [11] Zhang Y, Huang Z, Li K, Xie G, Feng Y, Wang Z, Li N, Liu R, Ding Y, Wang J, Yang J and Jia Z. TrkA promotes MDM2-mediated AGPS ubiquitination and degradation to trigger prostate cancer progression. J Exp Clin Cancer Res 2024; 43: 16.
- [12] Fu M, Li J, Xuan Z, Zheng Z, Liu Y, Zhang Z, Zheng J, Zhong M, Liu B, Du Y, Zhang L and Sun H. NDR1 mediates PD-L1 deubiquitination to promote prostate cancer immune escape via USP10. Cell Commun Signal 2024; 22: 429.
- [13] Li X and Song Y. Proteolysis-targeting chimera (PROTAC) for targeted protein degradation and cancer therapy. J Hematol Oncol 2020; 13: 50.
- [14] Li X, Pu W, Zheng Q, Ai M, Chen S and Peng Y. Proteolysis-targeting chimeras (PROTACs) in cancer therapy. Mol Cancer 2022; 21: 99.
- [15] Ross-Adams H, Lamb AD, Dunning MJ, Halim S, Lindberg J, Massie CM, Egevad LA, Russell R, Ramos-Montoya A, Vowler SL, Sharma NL, Kay J, Whitaker H, Clark J, Hurst R, Gnanapragasam VJ, Shah NC, Warren AY, Cooper CS, Lynch AG, Stark R, Mills IG, Grönberg H and Neal DE; CamCaP Study Group. Integration of copy number and transcriptomics provides risk stratification in prostate cancer: a discovery and validation cohort study. EBioMedicine 2015: 2: 1133-1144.
- [16] Latil A, Chêne L, Mangin P, Fournier G, Berthon P and Cussenot O. Extensive analysis of the 13q14 region in human prostate tumors: DNA analysis and quantitative expression of genes lying in the interval of deletion. Prostate 2003; 57: 39-50.
- [17] Wang L, Xi C, Zheng X, Huang Y, Xu H, Miao Y and Cheng Y. Familial 46, XY Disorder of Sexual Development identified in a Ph+BCR::ABL1 (P210+) Acute Lymphoblastic Leukemia septuagenarian female with RCBTB2::LPAR6 fusion gene: a case report. Front Oncol 2024; 14: 1339737.
- [18] Ke H, Wu Y, Wang R and Wu X. Creation of a prognostic risk prediction model for lung adenocarcinoma based on gene expression, methylation, and clinical characteristics. Med Sci Monit 2020; 26: e925833.
- [19] Kim JW, Moon SW, Mo HY, Son HJ, Choi EJ, Yoo NJ, Ann CH and Lee SH. Concurrent inactivating mutations and expression losses of RGS2, HNF1A, and CAPN12 candidate tumor suppressor genes in colon cancers. Pathol Res Pract 2023; 241: 154288.

- [20] Wu H, Wu Z, Li H, Wang Z, Chen Y, Bao J, Chen B, Xu S, Xia E, Ye D and Dai X. Glycosylphosphatidylinositol anchor biosynthesis pathway-based biomarker identification with machine learning for prognosis and T cell exhaustion status prediction in breast cancer. Front Immunol 2024; 15: 1392940.
- [21] Ge S, Zhang Q and Yang X. GPAA1 promotes the proliferation, invasion and migration of hepatocellular carcinoma cells by binding to RNAbinding protein SF3B4. Oncol Lett 2022; 23: 160.
- [22] Zhang H, Su J, Li B, Gao Y, Liu M, He L, Xu H, Dong Y, Zhang XC and Zhao Y. Structure of human glycosylphosphatidylinositol transamidase. Nat Struct Mol Biol 2022; 29: 203-209.
- [23] Mishra AK, Ye T, Banday S, Thakare RP, Su CT, Pham NNH, Ali A, Kulshreshtha A, Chowdhury SR, Simone TM, Hu K, Zhu LJ, Eisenhaber B, Deibler SK, Simin K, Thompson PR, Kelliher MA, Eisenhaber F, Malonia SK and Green MR. Targeting the GPI transamidase subunit GPAA1 abrogates the CD24 immune checkpoint in ovarian cancer. Cell Rep 2024; 43: 114041.
- [24] Zhang XX, Ni B, Li Q, Hu LP, Jiang SH, Li RK, Tian GA, Zhu LL, Li J, Zhang XL, Zhang YL, Yang XM, Yang Q, Wang YH, Zhu CC and Zhang ZG. GPAA1 promotes gastric cancer progression via upregulation of GPI-anchored protein and enhancement of ERBB signalling pathway. J Exp Clin Cancer Res 2019; 38: 214.
- [25] Niu X, You Q, Hou K, Tian Y, Wei P, Zhu Y, Gao B, Ashrafizadeh M, Aref AR, Kalbasi A, Cañadas I, Sethi G, Tergaonkar V, Wang L, Lin Y, Kang D and Klionsky DJ. Autophagy in cancer development, immune evasion, and drug resistance. Drug Resist Updat 2025; 78: 101170.
- [26] Silva JL, Foguel D, Ferreira VF, Vieira TCRG, Marques MA, Ferretti GDS, Outeiro TF, Cordeiro Y and de Oliveira GAP. Targeting biomolecular condensation and protein aggregation against cancer. Chem Rev 2023; 123: 9094-9138.
- [27] McGrail DJ, Garnett J, Yin J, Dai H, Shih DJH, Lam TNA, Li Y, Sun C, Li Y, Schmandt R, Wu JY, Hu L, Liang Y, Peng G, Jonasch E, Menter D, Yates MS, Kopetz S, Lu KH, Broaddus R, Mills GB, Sahni N and Lin SY. Proteome instability is a therapeutic vulnerability in mismatch repairdeficient cancer. Cancer Cell 2020; 37: 371-386, e312.

内蒙古自治区人民医院伦理委员会

202507204L

The Ethics Committee Approval of Inner Mongolia People's Hospital

The study, entitled "The ubiquitin ligase RCBTB2 regulates aggrephagy and inhibits prostate cancer progression by targeting GPAA1 for degradation" by Ren Mo et al. with clinical specimen data collection and animal experiments were performed with the approval of Ethics Committee of Inner Mongolia People's Hospital.

Ethics Committee

Inner Mongolia People's Hospital

Apr. 30-2025